Direct ab Initio Dynamics Calculations of the Reaction Rates for the Hydrogen Abstraction OH + HBr → H_2O + Br

Jing-yao Liu,*,† Ze-sheng Li,† Zhen-wen Dai,‡ Xu-ri Huang,† and Chia-chung Sun†

Institute of Theoretical Chemistry, State Key Laboratory of Theoretical and Computational Chemistry, Jilin University, Changchun 130023, P. R. China, and Department of Physics, Jilin University, Changchun 130023, P. R. China

Received: March 8, 2001; In Final Form: May 23, 2001

A direct dynamics study is carried out for the hydrogen abstraction reaction OH + HBr → H_2O + Br with a small barrier. The geometries and frequencies of all the stationary points are optimized by means of the three different methods, i.e., MP2/6-311G(d), BHLYP/6-311+G(d,p), and MP4SDQ/6-311G(d,p). It is shown that at the reactant side, there is a hydrogen-bonded complex (HBC) with an energy less than that of the reactants, and from the HBC to the products, the reaction system passes through a reactant-like transition state with an energy slightly higher than that of the reactants. To improve the reaction enthalpy and potential barrier, higher-level energies for the stationary points are made at the PMP4/6-311++G(3df,3pd) and CCSD(T)/6-311+G(2df,2p) levels. The potential energy profile is further refined by performing the CCSD(T) single-point energy calculations along the minimum-energy path (MEP) at the MP4SDQ level. Furthermore, the rate constants and activation energies over a wide range of temperatures 23−2000 K are evaluated by the improved canonical variational transition-state theory with a small-curvature tunneling correction. It is shown that the calculated rate constants are in agreement with the experiments at the temperature regions 249−416, 23−295, 76−242, and 230−360 K and at 1925 K, with a negative temperature dependence below 360 K, and that the variational effect should be considered for the rate constants at high temperatures. Moreover, the tunneling effects are found to contribute significantly to the rate constants at low temperatures.

Introduction

The reaction of the OH radical with HBr, which represents a neutral fast reaction with no apparent activation energy, is known to play a key role not only in stratospheric chemistry because it produces Br atoms which destroy the ozone very effectively,[1,2] but also in combustion chemistry, where it has been shown to contribute to the mechanism by which some brominated compounds act as fire retardants.[3] In the experimental studies, the rate constants were measured at room temperature (298 K),[4−7] at the temperature regions 249−416,[4] 23−295,[8] 76−242,[9] and 230−360 K,[10] and at a high temperature of 1925 K.[11] Also, the negative temperature dependence of the rate constants was reported below 295,[8] 150,[9] and 360 K.[10]

On the theoretical approaches, the reaction of OH + HBr has already been investigated by different theories[12−14] because of its relatively simple chemical system and interesting rate constants complexity. The statistical adiabatic capture theory[12] provided an upper limit to the experimental rate constant at very low temperatures and predicted the rate constant with the value of 3.5×10^{-10} cm^3 molecule^{-1} s^{-1} at 20 K but could not give accurate results for higher temperatures. The rotation bond approximation[15] was used in quantum scattering calculation[13] on the reaction OH + HBr → H_2O + Br for thermal collision energies. A simple potential energy surface (PES) was constructed for the reaction on the basis of a LEPS function and an accurate H_2O potential. It was shown that between the reactants and products, there is a transition state with an energy slightly less than that of the reactants. By means of the PES, the calculated rate constants for the reaction OH + HBr are in good agreement with the experimental values in the temperature range 23−295 K,[8] with a negative temperature dependence below 295 K. Furthermore, a quasiclassical trajectory (QCT)[14] calculation was performed with an empirical PES, which was a modification of the original PES used in the quantum scattering theory[13] just mentioned above, with parameters adjusted to fit the experimentally measured H_2O vibrational energy and the thermal rate constant. It was shown that for the reaction OH + HBr, the calculated rate constant at 300 K is in agreement with the experimental value which was estimated from the data over the temperature range 23−295 K.[8] In the calculation, the canonical variational transition state theory (VTST)[16,17] was used. Since the quantum scattering and the quasiclassical trajectory methods made use of nearly the same empirical potential energy surface, QCT also gave a transition state with an energy slightly less than that of the reactants.

In this paper, an attempt is made to investigate the dynamic properties of the hydrogen abstraction reaction OH + HBr by the direct dynamics method[18] over a wide range of temperatures, 23−2000 K. In this approach, the information on an accurate potential energy surface, including geometries, energies, gradients, and force constants of the stationary points and some extra points along the minimum energy path (MEP), is obtained directly from ab initio electronic structure calculations. It is shown that at the reactant side, there is a hydrogen-bonded complex (HBC) with an energy less than that of the reactants, and from HBC to products, the reaction system passes through a reactant-like transition state with an energy slightly higher than that of the reactants. Furthermore, the rate constants are

* Corresponding author.
† Institute of Theoretical Chemistry.
‡ Department of Physics.

10.1021/jp010879k CCC: $20.00
Published on Web 07/18/2001

calculated at the dynamic level of the VTST[16,17] together with the Polyrate8.0 program.[19] The improved canonical variational transition state theory (ICVT)[20] and the small-curvature tunneling (SCT) method[21] have been taken into account at the VTST level.

Calculation Methods

In the present study, all the electronic structure calculations are carried out by the Gaussian 98 program.[22] The energies, geometries and frequencies of the stationary points, in which the reactants, hydrogen-bonded complex (HBC), transition state (TS), and products are involved, are calculated at three levels: (i) the restricted or unrestricted second-order Moller-Pleset perturbation theory with the 6-311G(d) basis set (MP2/6-311G(d)); (ii) the hybrid Becke's half-and-half (BH) exchange with Lee−Yang−Parr (LYP) correlation functionals with the 6-311+G(d, p) basis set (BHLYP/6-311+G(d, p)); and (iii) the restricted or unrestricted fourth-order Moller-Pleset perturbation theory with single, double, and quadruple substitutions using the 6-311G(d, p) basis set (MP4SDQ/6-311G(d, p)). To yield more reliable reaction enthalpy and barrier height, single-point calculations for the stationary points are made at the CCSD(T)/6-311+G(2df,2p) level with the optimized geometries at the MP4SDQ/6-311G(d, p) level. Also, single-point calculations for the stationary points are made at the PMP4/6-311G++(3df,3pd) level with the optimized geometries at the MP2/6-311G(d) and BHLYP/6-311+G(d,p) levels. We denote the energies as CCSD(T)//MP4SDQ, PMP4//MP2, and PMP4//BHLYP, respectively. The minimum-energy path (MEP) is calculated by the intrinsic reaction coordinate (IRC) theory in mass-weighted Cartesian coordinates with a gradient step size of 0.05 $(amu)^{1/2}$ bohr at the MP4SDQ level. At the same level, the energy derivatives, including gradients and Hessians at geometries along the MEP, are obtained to calculate the curvature of the reaction path and to calculate the generalized vibrational frequencies along the reaction path. Furthermore, the energy profile is refined by higher-level energies at different selected points along MEP with the CCSD(T)/6-311+G(2df,2p) method.

By means of the Polyrate 8.0 program,[19] the theoretical rate constants and activation energies are calculated by using the improved canonical variational transition theory (ICVT)[20] with the small-curvature tunneling (SCT) approximation.[21] The two electronic states for OH reactant in the calculations of its electronic partition functions, with a 140 cm^{-1} splitting, are included. The Euler single-step integrator with a step size of 0.0001 $(amu)^{1/2}$ bohr is used to follow the MEP, and the generalized normal-mode analysis is performed every 0.01 $(amu)^{1/2}$ bohr. The curvature components are calculated by using a quadratic fit to obtain the derivative of the gradient with respect to the reaction coordinate.

Results and Discussion

1. Stationary Points. At the three different levels MP2/6-311G(d), BHLYP/6-311+G(d,p), and MP4SDQ/6-311G(d,p), the optimized geometric parameters of the reactants (OH and HBr), the hydrogen-bonded complex (HBC) (at the reactant side), the transition state (TS) (between HBC and products), and the product (H_2O) are computed as shown in Figure 1a. The bond lengths of the reactants and products agree with the experiment data[23] to within 1% at the MP2 level, 0.7% at the BHLYP level, and 0.2% at the MP4SDQ level. In the hydrogen-bonded complex, the O···H′ bond distances are 2.108 Å at the MP2 level, 2.115 Å at the BHLYP level, and 2.196 Å at the MP4SDQ level, and the other bond lengths (O−H and H′−Br)

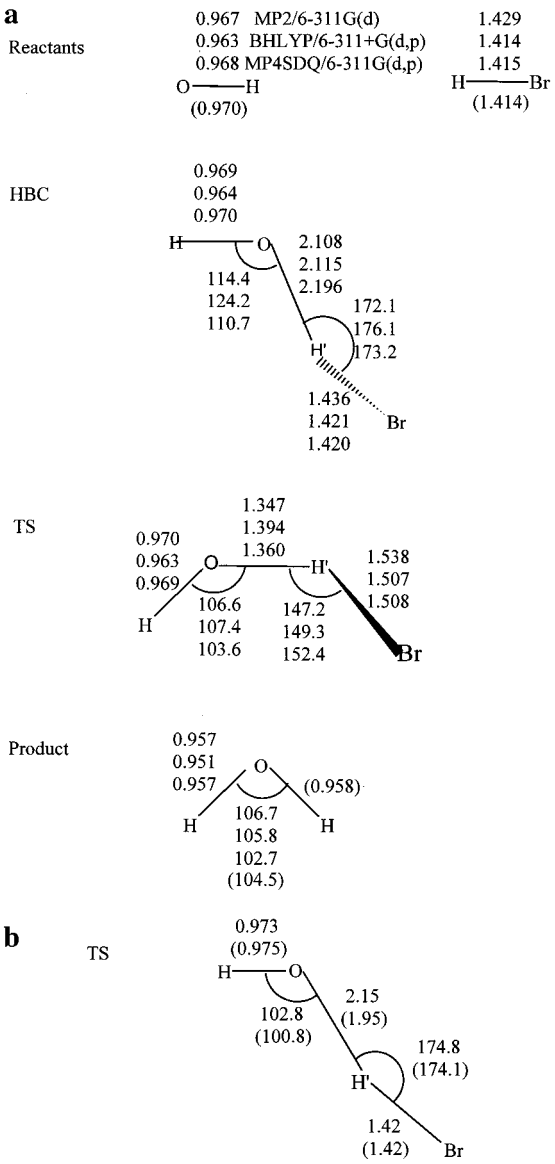

Figure 1. (a) Optimized geometric parameters (in Å and deg) of the reactants, hydrogen-bonded complex (HBC), transition state (TS), and products at the MP2/6-311G(d), BHLYP/6-311+G(d,p), and MP4SDQ/6-311G(d,p) levels, respectively. The values in the parentheses are the experimental values.[23] (b) The geometric parameters (in Å and deg) of the transition state (TS) with respect to the quantum scattering calculation[13] and the quasiclassical trajectory calculation[14] (in parentheses).

are very close to those of the reactants. For the transition state, at the MP2, BHLYP, and MP4SDQ levels, the calculations predict 40.51%, 46.59%, and 42.15% stretching of the O−H′ bond as compared to the O−H length in isolated H_2O. The calculations also predict 7.6%, 6.5%, and 6.6% stretching of the H′−Br bond as compared to the H−Br length in isolated HBr. The elongation of the forming bond (O−H′), which is greater than that of the breaking bond (H′−Br), indicates that the reaction proceeds via an "early" transition state, i.e., a reactant-like transition state. For the purpose of comparison, the geometric parameters of the transition states for the quantum scattering[13] and QCT[14] calculations are shown in Figure 1b (the geometric parameters of the reactants and products were not reported in the two papers[13,14]). The two transition states with almost linear O−H′−Br structures as shown in Figure 1b are quite different from our transition states with the bending O−H′−Br structure of about 150 ° shown in Figure 1a, while

TABLE 1: Calculated and Experimental Frequencies (cm^{-1}) of the Stationary Points

	MP2/6-311G(d)	BHLYP/6-311+G(d,p)	MP4SDQ/6-311G(d,p)	quantum scattering method[a]	QCT[b]	exptl[c]
OH	3794	3882	3818	3735	3735	3735
HBr	2629	2700	2702	2660	2660	2649
H_2O	3997, 3860, 1739	4088, 3984, 1653	4003, 3908, 1689	3756, 3652, 1595	3756, 3652, 1595	3756, 3657, 1595
HBC	3784, 2553, 409, 291, 176, 107,	3875, 2615, 367, 199, 168, 108	3805, 2657, 362, 264, 154, 99			
TS	3779, 1319, 815, 477, 251, 1692i	3882, 1390, 721, 413, 271, 1029i	3817, 1270, 730, 492, 211, 1403i	3670, 2584, 831, 216, 202	3626, 2521, 1038, 253, 235	

[a] Taken from ref 13. [b] Taken from ref 14. [c] Taken from ref 23.

TABLE 2: Relative Energies[a] and Enthalpies[b] (in kcal/mol) at Various Levels

	HBC		TS		H_2O + Br	
levels	ΔE	ΔE(0 K)	ΔE	ΔE(0 K)	ΔE	ΔH(298 K)
MP2	−4.19	−2.90	3.99	4.30	−33.80	−29.26
BHLYP	−3.21	−1.97	1.71	1.78	−28.51	−24.01
MP4SDQ	−3.58	−2.38	4.53	4.57	−29.92	−25.50
PMP4//MP2	−2.99	−1.70	1.46	1.77	−32.89	−28.35
PMP4//BHLYP	−2.97	−1.73	1.70	1.77	−32.86	−28.36
CCSD(T)// MP4SDQ	−2.91	−1.71	0.85	0.89	−32.72	−28.61
exptl[c]						−31.70
quantum scattering method[d]			−1.72	−0.12		
QCT[e]			−1.78	0.06		

[a] ΔE represents the relative energy without ZPE correction. ΔE(0 K) represents the relative energy with ZPE correction. [b] ΔH (298 K) represents the reaction enthalpy. [c] The experimental result of the heat of reaction from ref 23. [d] From ref 13. [e] From ref 14

the two transition states as shown in Figure 1b are rather similar to our hydrogen-bonded complex as shown in Figure 1a.

At the MP2, BHLYP, and MP4SDQ levels, the harmonic vibrational frequencies of all the stationary points are listed in Table 1. For the reactants and products, the largest deviations between the calculated and experimental harmonic frequencies[23] are 9% at the MP2 level, 9% at the BHLYP level, and 6% at the MP4SDQ level. For HBC, there are six harmonic vibrational frequencies. Since the geometrical variations between HBC and the reactants is small, it causes very little change in the harmonic vibrational frequencies of O−H and H′−Br in the complex, and the remaining four small harmonic vibrational frequencies characterize the vibrational motion of the complex. For the transition state, it is identified with one and only one imaginary frequency, and the imaginary frequencies take the values 1692i cm^{-1} at the MP2 level, 1029i cm^{-1} at the BHLYP level, and 1403i cm^{-1} at the MP4SDQ level. For the purpose of comparison, the frequencies of the reactants, transition states and products for the quantum scattering[13] and QCT[14] calculations are listed in Table 1 (the imaginary frequencies were not reported in the two papers[13,14]).

At the MP2, BHLYP, MP4SDQ, PMP4//MP2, PMP4//BHLYP and CCSD(T)//MP4SDQ levels, the relative energies (ΔE) of the HBC, the transition state, and the products with respect to the reactants are listed in Table 2. Also, the relative energies with ZPE corrections (ΔE(0 K)) of HBC and TS as well as the reaction enthalpies (ΔH(298 K)) are listed. For the three higher-level calculations PMP4//MP2, PMP4//BHLYP and CCSD(T)//MP4SDQ, one can find that the relative energies of HBC with ZPE correction are −1.7, −1.73, and −1.71 kcal/mol, respectively; i.e., the energy of HBC is less than that of the reactants OH + HBr, or equivalently, HBC is more stable than the reactants. At the three different higher levels, the reaction enthalpies take the values −28.35, −28.36, and −28.61 kcal/mol, respectively, and these values are about 3 kcal/mol larger than the experimental value of −31.70 kcal/mol which is obtained by the experimental standard heats of formation[23] (OH, 9.33 kcal/mol; HBr, −8.72 kcal/mol; H_2O, −57.85 kcal/mol; Br, 26.76 kcal/mol). At the three different higher levels, the relative energies of the transition state without ZPE correction are 1.46, 1.7, and 0.85 kcal/mol, respectively, while the relative energies with ZPE correction are 1.77, 1.77, and 0.89 kcal/mol, respectively. Note that the relative energy of TS is defined as the energy barrier of the reaction. At the CCSD(T)//MP4SDQ level, the energy barrier without ZPE correction is 0.85 kcal/mol, while the energy barrier with ZPE correction is 0.89 kcal/mol. For brevity, we only state without details that the energy barrier with ZPE correction or the energy barrier without ZPE correction at the CCSD(T)//MP4SDQ level is about 1 kcal/mol less than the other two barriers at the PMP4//MP2 and PMP4//BHLYP levels. Therefore, the reaction OH + HBr → H_2O +Br is nearly barrierless. For the purpose of comparison, the energy barrier for the quantum scattering calculation[13] is −1.72 (−0.12 with ZPE correction) kcal/mol, while the energy barrier for QCT[14] is −1.78 (0.06 with ZPE correction) kcal/mol (see Table 2).

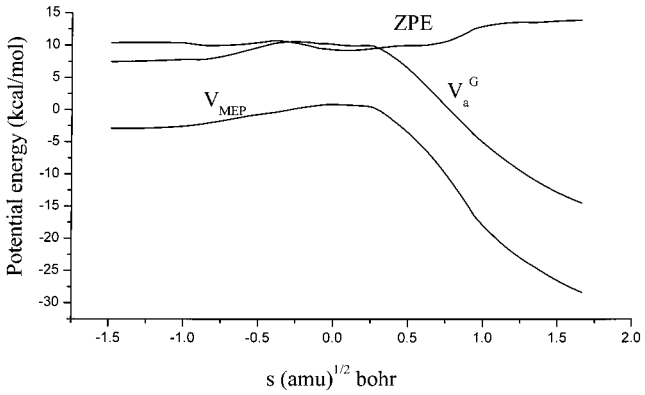

Figure 2. Classical potential energy curve (V_{MEP}), ground vibrationally adiabatic energy curve (V_a^G), and zero-point energy curve (ZPE) as functions of s (amu)$^{1/2}$ bohr at the CCSD(T)//MP4SDQ level.

2. Reaction Path Properties. In this paper, it is discussed that the minimum-energy path is obtained by the intrinsic reaction coordinate (IRC) theory at the MP4SDQ/6-311G(d, p) level and that the potential profile is further improved at the CCSD(T)/6-311+g(2df,2p) level. Figure 2 presents the classical potential energy curve ($V_{MEP}(s)$), the vibrationally adiabatic ground-state potential energy curve ($V_a^G(s)$), and the zero-point energy (ZPE) curve as a function of the intrinsic reaction coordinate (s) at the CCSD(T)//MP4SDQ level. As can be seen, the V_{MEP} and V_a^G curves are similar in shape, and the ZPE is practically constant as s varies, with only a gentle drop near the saddle point. To avoid a conceptual mistake of taking as a variational effect in the variational transition state rate calculations, a modification method[24] is applied to move the maximum

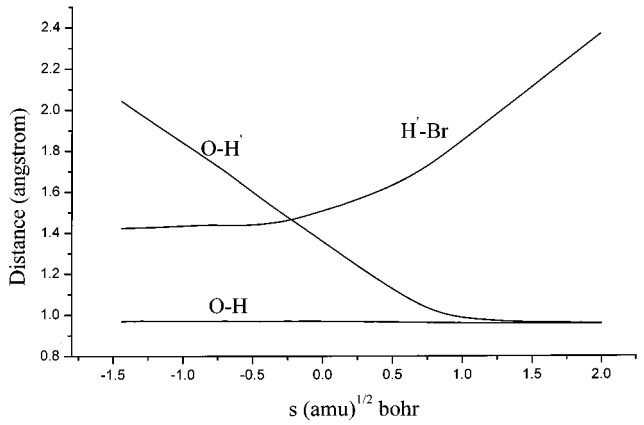

Figure 3. Changes of the bond lengths (in Å) as functions of s (amu)$^{1/2}$ bohr at the MP4SDQ/6-11G(d,p) level.

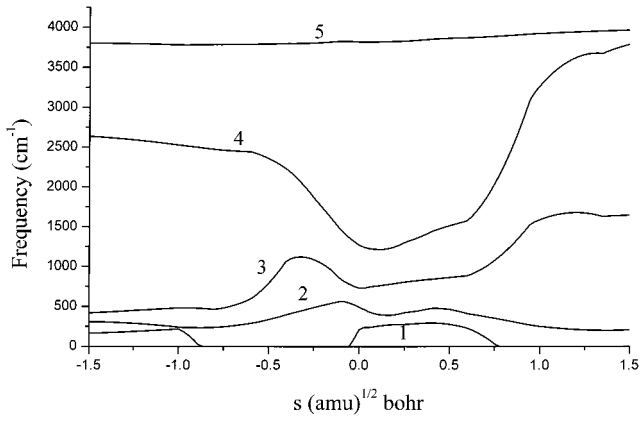

Figure 4. Changes of the generalized normal-mode vibrational frequencies as functions of s (amu)$^{1/2}$ bohr at the MP4SDQ/6-311G-(d,p) level.

of the CCSD(T)//MP4SDQ potential energy curve to its original position ($s = 0$ for the MP4SDQ level), and the shifted curve is used as our electronic PES. Note that the location of the maximum on the potential energy curve $V_{MEP}(s)$ at the CCSD-(T)//MP4SDQ level is shifted toward the reactants to approximately $s = -0.25$ (amu)$^{1/2}$ bohr. In Figure 2, the $V_{MEP}(s)$ actually represents the shifted curve.

Figure 3 describes the structure changes of the bond length along the IRC. It appears that the O−H bond distance is almost invariable during the reaction process and that the active O−H′ and H′−Br bonds change strongly during the course of the hydrogen abstraction reaction. The H′−Br bond, which is broken, elongates after about $s = -0.5$ (amu)$^{1/2}$ bohr. The O−H′ bond distance decreases smoothly to the O−H bond distance of 0.975 Å in H_2O at about $s = 1.2$ (amu)$^{1/2}$ bohr. It is thus evident that the geometric changes mainly take place in the region of $s = -0.5-1.2$ (amu)$^{1/2}$ bohr on the IRC.

The variation of the generalized normal-mode vibrational frequencies along the IRC is drawn in Figure 4. In the negative limit of s ($s = -\infty$), the frequencies correspond to those of HBC, and in the positive limit of s ($s = +\infty$), the frequencies are associated with the product (H_2O). Most of these frequencies do not change significantly in going from the reactants to products. The frequency of mode 5 correlating with the O−H stretching vibration is almost unchanged in the whole process, and mode 3 transforms to the bending vibration mode of H_2O in the products side. The two lowest harmonic frequencies (mode 1 and 2) are the transitional modes, which correspond to free rotations and translations that evolve into vibrations.

TABLE 3: Rate Constants (cm^3 molecule^{-1} s^{-1}) for the Temperature Range 23−2000 K

T(K)	ICVT	ICVT/SCT	exptl
23	2.14×10^{-21}	1.19×10^{-10}	$(1.07 \pm 0.04) \times 10^{-10}$ [a]
30.5	8.42×10^{-19}	6.41×10^{-11}	$(8.78 \pm 0.44) \times 10^{-11}$ [a]
44	1.89×10^{-16}	2.96×10^{-11}	$(7.87 \pm 0.27) \times 10^{-11}$ [a]
52	1.14×10^{-15}	2.12×10^{-11}	$(5.54 \pm 0.15) \times 10^{-11}$ [a]
75	2.01×10^{-14}	1.06×10^{-11}	$(4.83 \pm 0.22) \times 10^{-11}$ [a]
76	2.18×10^{-14}	1.03×10^{-11}	$(2.9 \pm 0.9) \times 10^{-11}$ [b]
92	6.08×10^{-14}	7.44×10^{-12}	$(3.0 \pm 0.5) \times 10^{-11}$ [b]
107	1.16×10^{-13}	5.86×10^{-12}	$(2.0 \pm 0.3) \times 10^{-11}$ [b]
133	2.38×10^{-13}	4.30×10^{-12}	$(1.6 \pm 0.2) \times 10^{-11}$ [b]
147	3.11×10^{-13}	3.80×10^{-12}	$(1.4 \pm 0.1) \times 10^{-11}$ [b]
169	4.28×10^{-13}	3.26×10^{-12}	$(1.5 \pm 0.3) \times 10^{-11}$ [b]
170	4.33×10^{-13}	3.24×10^{-12}	$(2.97 \pm 0.46) \times 10^{-11}$ [a]
173	4.49×10^{-13}	3.19×10^{-12}	$(0.8 \pm 0.1) \times 10^{-11}$ [b]
194	5.60×10^{-13}	2.89×10^{-12}	$(1.5 \pm 0.4) \times 10^{-11}$ [b]
222	6.99×10^{-13}	2.62×10^{-12}	$(1.3 \pm 0.2) \times 10^{-11}$ [b]
230	7.39×10^{-13}	2.57×10^{-12}	$(1.46 \pm 0.17) \times 10^{-11}$ [c]
242	7.95×10^{-13}	2.50×10^{-12}	$(1.1 \pm 0.1) \times 10^{-11}$ [b]
243	8.00×10^{-13}	2.50×10^{-12}	$(1.2 \pm 0.14) \times 10^{-11}$ [c]
249	8.26×10^{-13}	2.47×10^{-12}	$(1.31 \pm 0.08) \times 10^{-11}$ [d]
260	8.76×10^{-13}	2.42×10^{-12}	$(1.12 \pm 0.13) \times 10^{-11}$ [c]
273	9.34×10^{-13}	2.38×10^{-12}	$(1.22 \pm 0.05) \times 10^{-11}$ [d]
278	9.56×10^{-13}	2.37×10^{-12}	$(1.20 \pm 0.13) \times 10^{-11}$ [c]
295	1.03×10^{-12}	2.34×10^{-12}	$(1.16 \pm 0.04) \times 10^{-11}$ [a]
298	1.04×10^{-12}	2.34×10^{-12}	$(1.11 \pm 0.07) \times 10^{-11}$ [d]
326	1.16×10^{-12}	2.32×10^{-12}	$(1.18 \pm 0.08) \times 10^{-11}$ [d]
328	1.17×10^{-12}	2.32×10^{-12}	$(1.05 \pm 0.12) \times 10^{-11}$ [c]
360	1.30×10^{-12}	2.32×10^{-12}	$(0.97 \pm 0.14) \times 10^{-11}$ [c]
369	1.33×10^{-12}	2.32×10^{-12}	$(1.12 \pm 0.05) \times 10^{-11}$ [d]
416	1.51×10^{-12}	2.36×10^{-12}	$(1.21 \pm 0.10) \times 10^{-11}$ [d]
500	1.85×10^{-12}	2.53×10^{-12}	
600	2.29×10^{-12}	2.86×10^{-12}	
800	3.37×10^{-12}	3.83×10^{-12}	
1000	4.74×10^{-12}	5.15×10^{-12}	
1500	9.52×10^{-11}	9.89×10^{-12}	
1925	1.51×10^{-11}	1.55×10^{-11}	2.65×10^{-11} [e]
2000	1.63×10^{-11}	1.66×10^{-11}	

[a] Values from ref 8 (23−295 K). [b] Values from ref 9 (76−242 K). [c] Values from ref 10 (230−360 K). [d] Values from ref 4 (249−416 K). [e] The value from ref 11 (1925K).

Their maximum appears near the transition state and fall to zero toward reactants and products. Of all the frequencies, the frequency of mode 4, which represents the evolution from the stretching vibrational frequency of HBr to the frequency of the O−H stretching vibration of H_2O, has a significant change in the region from $s = -0.5$ to 1.2 (amu)$^{1/2}$ bohr as the reaction proceeds. Therefore, mode 4 can be referred to as the "reactive mode" in the reaction. Moreover, the dramatic drop of the mode 4 near the saddle points is compensated partially by the two transitional modes; as a result, the ZPE shows small variations with s.

3. Rate Constants Calculation. The potential energy information is put into the POLYRATE 8.0 program[19] to produce the VTST[16,17] rate constants over a wide temperature range, 23−2000 K. The forward rate constants are calculated by the improved variational transition state theory[20] with a small-curvature tunneling correction[21] (ICVT/SCT). The ICVT and ICVT/SCT rate constants together with the experimental data obtained from Ravishankara et al.[4] (249−426 K), from Sims et al.[8] (23−295 K), from Atkinson et al.[9] (76−242 K), from Bedjanian et al.[10] (230−360 K), and from Wilson et al.[11] (1925 K) are listed in Table 3. The comparison of the theoretical rate constants with experimental values is plotted in Figure 5. For brevity, we only state without details that (1) since the OH + HBr reaction has a hydrogen-bonded complex with a potential energy less than that of the reactants, the reaction has two variational transition states, i.e., an outer one that occurs as OH

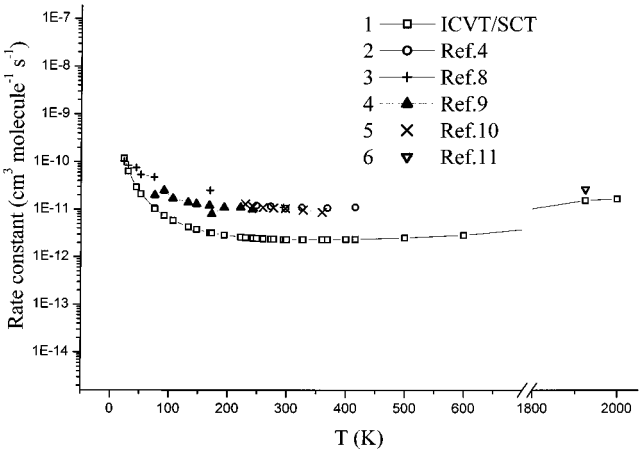

Figure 5. Rate constants (cm^3 molecule^{-1} s^{-1}) as functions of the temperature (K) over the temperature range 23−2000 K.

and HBr come together to form the hydrogen-bonded complex and an inner variational transition state near the potential energy barrier and that (2) as the free energy barrier of the inner TS is much higher than that of the outer TS, the rate for the reaction is controlled by the inner TS. Thus, the improved canonical variational transition state theory (ICVT) can be used for the calculation of the rate constants.

For this reaction, the dynamical bottleneck location, which refers to the optimized location of the dividing surface, remains close to the saddle point over the temperature range 23−369 K with a value from −0.0004 (amu)$^{1/2}$ bohr at 23 K to 0.0104 (amu)$^{1/2}$ bohr at 369 K, while at high temperatures ($T \geq 400$ K), the location is at about 0.25 (amu)$^{1/2}$ bohr. The bottleneck properties indicate that the variational effect is small in the low temperature range and should be considered at high temperatures. Besides, from Table 4, it is obviously seen that the SCT contribution has a greater influence on the rate constants. The ratio of the ICVT/SCT rate constant and the ICVT rate constant is a value of 1.1−4 in the range 800−222 K and becomes particularly significant at ultralow temperatures. The values of ratios are 5.6×10^{10} at 23 K, 4.7×10^{2} at 76 K, 50 at 107 K, and 5.6 at 194 K. Therefore, it is shown that the tunneling plays an important role in the reaction, especially in the low-temperature range.

The ICVT/SCT rate constants are in agreement with the experimental values[4,8−11] in the measured temperature ranges. The ICVT/SCT rate constant is only 1.1 times the experimental one at 23 K.[8] In the temperature region 30.5−52 K, the calculated values underestimate the experimental data of Sims et al.[8] by a factor of 1.3−2.6, and in 75−416 K range, they are a factor of 2.8−5 lower than the corresponding experimental values.[8−10] The *k*(exptl):*k*(ICVT/SCT) ratio is 1.7 at 1925 K. Furthermore, the calculated rate constants exhibit the negative temperature dependence below 360 K. This result agrees well with that of Bedjanian et al.[10] However, it is different from that of Atkinson et al.[9] and Sims et al.,[8] who predicted the negative temperature dependence below 150 and 295 K, respectively. It can be noted also that the measured values of $(4.83 \pm 0.22) \times 10^{-11}$ cm^3 molecule^{-1} s^{-1} at 75 K and $(2.97 \pm 0.46) \times 10^{-11}$ cm^3 molecule^{-1} s^{-1} at 170 K from Sims et al.[8] are about 2 times higher than those from Atkinson et al.[9] at 76 and 169 K, respectively, whereas our results are much close to those of Atkinson.[9]

The values of the computed activation energy based on the ICVT/SCT method in several different temperature regions are near zero, only −0.19, 0.38, and 1.75 kcal/mol for the regions 23−360, 360−600, and 600−1000 K, respectively. The activation energy takes a negative value in 23−360 K; as a consequence, the rate constants show the negative temperature dependence. The activation energy increases as the temperature increases. The calculation results are in line with the experimental results[4,5] that the reaction of OH +HBr has no apparent activation energy.

For the quantum scattering[13] calculation, the calculated rate constants as shown in Figure 10 in the ref 13 are in good agreement with the experimental values in the temperature range 23−295 K,[8] with a negative temperature dependence below 295 K. Furthermore, for the quasiclassical trajectory[14] calculation, the calculated rate constant of 1.6×10^{-11} cm^3 molecule^{-1} s^{-1} at 300 K is in agreement with the experimental value of 1.1×10^{-11} cm^3 molecule^{-1} s^{-1}.[8]

Conclusion

In the present study, a direct dynamic study for the hydrogen abstraction reaction of OH + HBr has been carried out by means of ab initio calculations. The reaction proceeds via a hydrogen-bonded complex and then a transition state. The PES information is obtained at the MP4SDQ/6-311G(d,p) level, and higher-level energies at the stationary points and along the reaction path are calculated by the CCSD(T)/6-311+G(2df,2p) method. At the CCSD(T)//MP4SDQ level, the calculated reaction enthalpy is slightly lower than the experimental value, and the activation energy is near zero. The changes of the geometry and generalized normal-mode vibrational frequencies along the IRC mainly take place in the region from $s = -0.5$ to 1.2 (amu)$^{1/2}$ bohr. The ICVT/SCT rate constants are in agreement with the experimental ones and show the negative temperature dependence below 360 K. The variational effect is small at low temperatures and should be taken into account at high temperatures. The small-curvature tunneling plays an important role particularly in the low-temperature range.

Acknowledgment. We would like to thank Professor Donald G. Truhlar for his provision of the POLYRATE 8.0 program. This work is supported by the National Natural Science Foundation of China (G29892168, 200073014), Doctor Foundation by the Ministry of Education, Foundation for University Key Teacher by the Ministry of Education, and Key Subject of Science and Technology by the Ministry of Education of China.

References and Notes

(1) DeMorse, W. B.; Sander, S. P.; Golden, D. M.; Molina, M. J.; Hampson, R. F.; Kurylo. M.; Howard, C. J.; Ravishankara, A. R. *Chemical Kinetics and Photochemical Data for use in Stratospheric Modeling, Evaluation Number 9*; JPL Publication 90-1; Jet Propulsion Laboratory, California Institute of Technology: Pasadena, CA, 1990.

(2) Wayne, R. P. *Chemistry of Atmospheres*, 2nd ed.; Oxford University Press: New York, 1993; p 165.

(3) Clark, D. R.; Simmons, R. F.; Smith, D. A. *Trans. Faraday Soc.* **1970**, *66*, 1423.

(4) Ravishankara, A. R.; Wine, P. H.; Langford, A. O. *Chem. Phys. Lett.* **1979**, *63*, 479.

(5) Ravishankara, A. R.; Wine, P. H.; Wells, J. R. *J. Chem. Phys.* **1985**, *83*, 447.

(6) Cannon, B. D.; Robertshaw, J. S.; Smith, I. W. M.; Williams, M. D. *Chem. Phys. Lett.* **1984**, *105*, 380.

(7) Jourdain, J. L.; Le Bras, G.; Combourieu, J. *Chem. Phys. Lett.* **1981**, *78*, 483.

(8) Sims, I. R.; Smith, I. W. M.; Clary, D. C.; Bocherel, P.; Rowe, B. R. *J. Chem. Phys.* **1994**, *101*, 1748.

(9) Atkinson, D. B.; Jaramillo, V. I.; Snith, M. A. *J. Phys. Chem. A* **1997**, *101*, 3356.

(10) Bedjianian, Y.; Riffault, V.; bras, G. Le; Poulet, G. *J. Photochem. Photobiol., A: Chem.* **1999**, *128*, 15.

(11) Wilson, W. E., Jr.; Donovan, J. T.; Fristrom, R. M. *12th Symp. Combust.* **1969**, 929.

(12) Clary, D. C.; Stoecklin, T. S.; Wickham, A. G. *J. Chem. Soc., Faraday Trans*. **1993**, *89*, 2185.
(13) Clary, D. C.; Nyman, G.; Hernandez, R. *J. Chem. Phys*. **1994**, *101*, 3704.
(14) Nizamov, B.; Setser, D. W.; Wang, H.; Peslherbe, G. H.; Hase, W. L. *J. Chem. Phys*. **1996**, *105*, 9897.
(15) Clary, D. C. *J. Chem. Phys*. **1991**, *95*, 7298.
(16) Truhlar, D. G.; Garrett, B. C. *Acc. Chem. Res*. **1980**, *13*, 440.
(17) Truhlar, D. G.; Isaacson, A. D.; Garrett, B. C. Generalized Transition State Theory. In *The Theory of Chemical Reaction Dynamics*; Baer, M., Ed.; CRC Press: Boca Raton, FL, 1985; Vol. 4. p 65.
(18) (a) Truhlar, D. G. Direct Dynamics Method for the Calculation of Reaction Rates. In *The Reaction Path in Chemistry: Current Approaches and Perspectives*; Heidrich, D., Ed.; Kluwer: Dordrecht, The Netherlands, 1995; pp 229−255. (b) Truhlar, D. G.; Garrett, B. C.; Klippenstein, S. J. *J. Phys. Chem*. **1996**, *100*, 12771. (c) Hu, W. P.; Truhlar, D. G. *J. Am. Chem. Soc*. **1996**, *118*, 860.
(19) Chang, Y. Y.; Corchado, J. C.; Fast, P. L.; Villa, J.; Hu, W. P.; Liu, Y. P.; Lynch, G.. C.; Jackels, C. F.; Nguyen, K. A.; Gu, M. Z.; Rossi, I.; Coitino, E. L.; Clayton, S.; Melissas, V. S.; Lynch, B. J.; Steckler, R.; Garrett, B. C.; Isaacson, A. D.; Truhlar, D. G. *POLYRATE*, version 8.0; University of Minnesota: Minneapolis, MN, 1998.
(20) Garrett, B. C.; Truhlar, D. G.; Grev, R. S.; Magnuson, A. W. *J. Phys. Chem*. **1980**, *84*, 1730.
(21) Lu, D. H.; Truong, T. N.; Melissas, V. S.; Lynch, G. C.; Liu, Y. P.; Garrett, B. C.; Steckler, R.; Issacson, A. D.; Rai, S. N.; Hancock, G. C.; Lauderdale, J. G.; Joseph, T.; Truhlar, D. G. *Comput. Phys Commun*. **1992**, *71*, 235.
(22) Frisch, M. J.; Truck, G. W.; Schlegel, H. B.; Scuseria, G. E.; Robb, M. A.; Cheeseman, J. R.; Zakrzewski, V. G.; Montgomery, J. A., Jr.; Stratmann, R. E.; Burant, J. C.; Dapprich, S.; Millam, J. M.; Daniels, A. D.; Kudin, K. N.; Strain, M. C.; Farkas, O.; Tomasi, J.; Barone, V.; Cossi, M.; Cammi, R.; Mennucci, B.; Pomelli, C.; Adamo, C.; Clifford, S.; Ochterski, J.; Petersson, G. A.; Ayala, P. Y.; Cui, Q.; Morokuma, K.; Malick, D. K.; Rabuck, A. D.; Raghavachari, K.; Foresman, J. B.; Cioslowski, J.; Ortiz, J. V.; Boboul, A. G.; Stefnov, B. B.; Liu, G.; Liaschenko, A.; Piskorz, P.; Komaromi, L.; Gomperts, R.; Martin, R. L.; Fox, D. J.; Keith, T.; Al-Laham, M. A.; Peng, C. Y.; Nanayakkara, A.; Gonzalez, C.; Challacombe, M.; Gill, P. M. W.; Johson, B.; Chen, W.; Wong, M. W.; Andres, J. L.; Gonzalez, C.; Head-Gordon, M.; Replogle, E. S.; Pople, J. A. *Gaussian 98*, revision X.; Gaussian, Inc.: Pittsburgh, PA, 1998.
(23) Chase, M. W., Jr. *NIST-JANAF Themochemical Tables, Fourth Edition. J. Phys. Chem. Ref. Data* **1998**, Monograph 9.
(24) Garcia, J. E.; Corchado, J. C. *J. Phys. Chem*. **1995**, *99*, 8613.